Journal of Saudi Chemical Society (2014) **18**, 291–298

King Saud University

Journal of Saudi Chemical Society

www.ksu.edu.sa
www.sciencedirect.com

ORIGINAL ARTICLE

Photocatalytic reduction of nitrate over TiO_2 and Ag-modified TiO_2

Krisana Kobwittaya, Sanya Sirivithayapakorn *

Department of Environmental Engineering, Faculty of Engineering, Kasetsart University, Bangkok 10900, Thailand

Available online 21 February 2014

KEYWORDS

Denitrification;
Formic acid;
Hole scavenger;
Thin film;
Stoichiometric

Abstract This research work presents the efficiency of the TiO_2 and Ag–TiO_2 thin films prepared by the sol–gel method and coated onto the surface of 304 stainless steel sheets used in the photocatalytic nitrate reduction processes. The Ag–TiO_2 thin films had the weight by weight (w/w) ratio of Ag^+/TiO_2 of 0.1% as Ag atom. The XRD results showed that the crystalline phase structure of TiO_2 on the Ag–TiO_2 thin films was anatase. The optical band gaps of the TiO_2 and 0.1% Ag–TiO_2 thin films were respectively 3.27 and 2.70 eV, while the surface of the prepared catalysts was hydrophobic with the respective average water contact angles of 94.8° and 118.5° for the TiO_2 and 0.1% Ag–TiO_2 thin films. The net efficiencies of photocatalytic nitrate reduction of TiO_2 and 0.1% Ag–TiO_2 were 41.4% and 70.0%, respectively. The loading of Ag only influenced the nitrate removal efficiency without affecting the stoichiometric ratio of formate to nitrate. The net stoichiometric ratio of formate to nitrate of all experiments was 2.8:1.0, which is close to the stoichiometric ratio of 2.5:1.0 of the nitrate reduction to nitrite and then to nitrogen gas.

1. Introduction

A number of research studies have reported that the photocatalytic reduction of nitrate in the aqueous solution could be achieved with high efficiency using various types of photocatalysts. Of various photocatalysts, titanium dioxide (TiO_2) and TiO_2 modified with various co-catalysts, such as iron and silver, were found to be the most efficient for nitrate reduction with high selectivity toward the reaction pathway that generates nitrogen gas, which is a harmless by-product (Anderson [1]).

Most existing research works on the photocatalytic nitrate reduction used the suspended photocatalysts in the aqueous solution. Nonetheless, if the reuse of the photocatalysts is planned this method presents itself with a major drawback as it requires additional processes, such as filtration or centrifugation, to separate and retrieve the photocatalysts from the aqueous solution. Meanwhile, many other studies reported that photocatalysts coated as a thin film on the surfaces of materials were suitable for the treatment or removal of pollutants in the gas–solid phase [15,17,24]. The thin film photocatalysts are nevertheless infrequently used for the photoreaction in the aqueous solution since the thin film photocatalysts might not be as effective as those suspended in the aqueous solution. This is mainly because only a portion of the surface

* Corresponding author. Tel.: +66 2 9428555x1013; fax: +66 2 5790730.
E-mail addresses: g5514501485@ku.ac.th (K. Kobwittaya), sanya.si@ku.ac.th (S. Sirivithayapakorn).

Peer review under responsibility of King Saud University.

ELSEVIER Production and hosting by Elsevier

http://dx.doi.org/10.1016/j.jscs.2014.02.001

area of the thin film photocatalysts is exposed to the target substances, thereby limiting the amount of photocatalysts that could take part in the reaction [9].

Another requirement of the photocatalytic nitrate reduction processes is the addition of simple organic compounds which would act as an electron hole scavenger that provides electrons to fill the electron holes in the valence band. Previous studies reported that formic acid is one of the most efficient hole scavengers for nitrate reduction over TiO_2 [5,21,24].

This research study aims to demonstrate the efficiency of the coated TiO_2 and Ag–TiO_2 in photocatalytic nitrate reduction with formic acid as the hole scavenger and UV-A as photo energy. In this work, TiO_2 and Ag–TiO_2 prepared by the simplified sol–gel technique were separately coated to form thin films on the surface of stainless steel sheets. The reason why we chose 304 stainless steel sheets is because it has good combination of strength and plasticity, excellent corrosion resistance, and it has been used widely in many industrial applications. The physical properties of the thin film photocatalysts, including crystalline phases of TiO_2, surface morphology, composition of the thin films, contact angles and band gaps, are detailed. By providing large surface area of the coated catalyst films in our system, the issue of low performance due to the limited catalyst amount for the photo reaction could be solved and a better performance was achieved.

2. Experiment

2.1. Materials

The chemicals used in this study were titanium tetraisopropoxide (TTIP, >99.999%, Sigma–Aldrich) as the TiO_2 source and isopropanol (C_2H_7O, >99.5%, Sigma–Aldrich) as the solvent for the preparation of TiO_2 nanoparticle. Silver nitrate ($AgNO_3$, >99%, Sigma–Aldrich) was used as the Ag source. Hydrochloric acid (HCl, 37%, Merck) and nitric acid (HNO_3, 65%, Merck) were used to adjust pH for the preparation of TiO_2 and Ag–TiO_2 sol–gel solution. Potassium nitrate (KNO_3, >99%, Merck) was used as the nitrate source while formic acid (HCOOH, >95%, Sigma–Aldrich) was used as the formate source. The solutions were prepared using deionized water.

2.2. Methods

2.2.1. Preparation of TiO_2 and Ag–TiO_2

The TiO_2 thin films were prepared by dip coating the acid catalyzed sol–gel with TTIP as a precursor onto the surface of 304 stainless steel sheets ($40.0 \times 85.0 \times 0.3$ mm) according to the processes described by Rojviroon et al. [19]. For the preparation of Ag–TiO_2 thin films, silver nitrate ($AgNO_3$) solution (prepared by dissolving $AgNO_3$ in deionized water) was added into the original acid catalyzed sol–gel used for the preparation of the TiO_2 thin films, with the w/w ratio of Ag^+/TiO_2 of 0.1% as Ag atom. Afterward, the solution pH was adjusted with concentrated nitric acid to the 2–3 pH range. The solution was then stirred at room temperature in a coating chamber [20] with constant flow of nitrogen gas for 1 h before use. Subsequently, the Ag^+/TiO_2 sol–gel solution was coated onto the stainless steel sheets according to the method described by Rojviroon et al. [19]. In this research study, the coating of TiO_2 and Ag–TiO_2 to form thin films on the surface of stainless steel sheets comprised of 5 layers each.

2.2.2. Characterization of the photocatalysts

The X-ray diffraction (XRD) patterns were obtained from samples of the stainless steel sheets coated with 0.1% Ag–TiO_2 with a Bruker model D8 Advance equipped with a Cu Kα radiation at a scan rate of $0.02^\circ\ s^{-1}$. To verify the composition of the thin films, the elemental analysis was performed using X-ray Fluorescence (XRF) (Horiba XGT-2000 W) with the X-ray tube and the current parameters set to 15 kV and 1 mA.

The optical band gap of the thin films was determined with a UV–Vis diffuse reflectance spectroscopy (DRS) in the 290–800 nm range of wavelength (Lamda 650 Perkin Elmer) equipped with a 150 mm diameter Spectralon integrating sphere. To estimate the band gap energies, the absorption onsets of the samples were determined by linear extrapolation from the inflection point of the curve to the baseline (Ge et al. [8], [3]). The band gap, E_g, was obtained from a linear regression of $(\alpha h\nu)^{1/2}$ against $h\nu$ with extrapolation to zero (Eq.(1), often called a Tauc plot) (e.g. [22,23]).

$$(\alpha h\nu)^{1/2} = A(h\nu - E_g) \quad (1)$$

where α is the absorbance, unitless; $h\nu$ is photon energy, eV; A is an independent parameter of the photon energy for the respective transitions, eV; E_g is the band gap, eV.

The surface properties of the thin films were examined by the Atomic Force Microscopy (AFM) technique (Asylum research MFP-3D-BIO™). The surface area of the thin films and the root mean square (RMS) average roughness were determined by the Gwyddion software program, version 2.22 (http://gwyddion.net). The grain size was measured directly from cross sectional AFM images at the base of each grain.

The changes of the water contact angles were monitored by the sessile drop method (Surface Energy Evaluation (SEE) System, Advex Instruments). Static contact angle measurements by the sessile drop method were measured using a set of standard testing liquids at ambient temperature, 22 °C and 60% relative humidity. The data analysis was performed via SEE System software. Each resulting contact angle was an average of 5 measured values that were recorded 30 s after reposing each drop of 5 μL volume on the sample surface.

2.2.3. Photocatalytic activity test

Photocatalytic reactions were performed in the photoreactor (Fig. 1) fabricated from a 5-L cylindrical borosilicate glass of 3 mm thick with the working volume of 4.5 L. The reactor was irradiated with three 15 W black-light bulbs. Black-light bulbs, i.e. UV-A bulbs, were selected as the light source in this study as they are less hazardous and produce less heat in comparison with the mercury and xenon lamps. In addition, the stoichiometric requirements for formate are reported for both TiO_2 and Ag–TiO_2 thin films. After filling the reactor with the synthetic solutions, the average UV light intensity in the photoreactor was 125 $\mu W/m^2$. The light intensity was measured by UV-light meter (Model UV-340) at the center of the rector. The top and the bottom parts of the reactor were made of acrylic. Inside the reactor, twelve coated stainless steel sheets were mounted at three locations, with four sheets at each

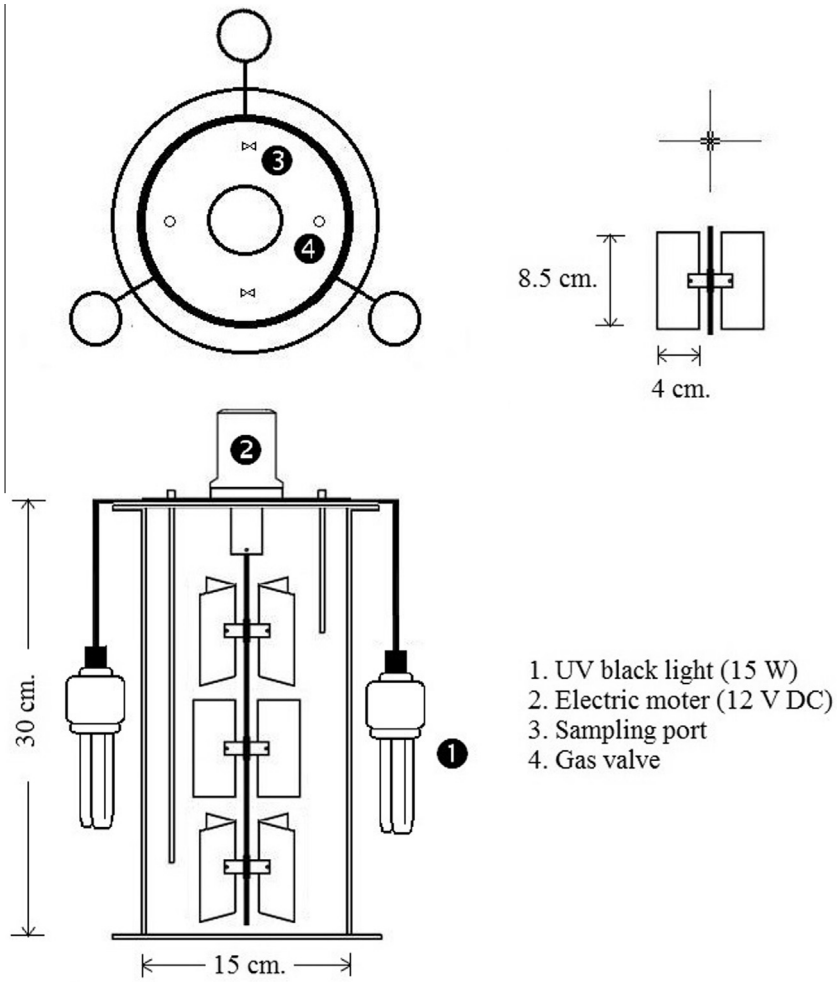

Figure 1 The schematic of the photoreactor for nitrate reduction.

location, along the shaft that was powered by a motor (Fig. 1). The coated stainless steel sheets acted as the photocatalyst surfaces as well as mixing paddles. Throughout the experiment, the motor velocity was maintained at 60 rpm. The top cover contained two gas valves and two sampling ports. The first gas valve was used to feed nitrogen gas to displace oxygen while the second gas valve was used to release gases out of the reactor. The water samples were collected from the two sampling ports that withdraw water from two different depths. The analytical results of the water samples from both levels were averaged and used as the representative results of the entire reactor.

The synthetic water was prepared by added potassium nitrate and formic acid (i.e. the hole scavenger) in deionized water. The initial concentrations of nitrate and formic acid were 7.14–59.3 mM, respectively, to provide the initial ratio of formate to nitrate of 8 to 1, as per the stoichiometric ratio described by Rengaraj and Li [18]. Water samples were periodically collected every 30 min from the beginning of the experiment until 360 min. The concentrations of nitrate, nitrite, ammonium and formate in the water samples were measured with the Dionex DX-120; AS12A column, Dionex IonPac CS10 column, Dionex IonPac; AS11-HC column ion chromatography, respectively.

Two additional sets of control experiments were also carried out. The first set was the experiments in which the uncoated stainless steel sheets were employed to verify whether the nitrate reduction could occur under only UV light without the photocatalysts. Meanwhile, the second set involved the experiments with UV light and both types of catalysts (i.e. TiO_2 and Ag–TiO_2) under the normal experimental conditions except that no nitrate was added to the synthetic water to determine the loss of formic acid from the system due to the photocatalytic process.

The nitrogen selectivity $S(N_2)$ was calculated from the balance of nitrogen by-products (NO_2^- and NH_4^+) analyzed in solution, according to Eqs. (2)–(4) [6].

$$S(NO_2^-) = [NO_2^-]/([NO_3^-]_0 - [NO_3^-]_t) \quad (2)$$

$$S(NH_4^{+-}) = [NH_4^+]/([NO_3^-]_0 - [NO_3^-]_t) \quad (3)$$

$$S(N_2) = ([NO_3^-]_0 - [NO_3^-]_t - [NO_2^-]_t - [NH_4^+]_t)/([NO_3^-]_0 - [NO_3^-]_t) \quad (4)$$

where $[X]_0$ is the concentration at time = 0 and $[X]_t$ is the concentration at time = t.

In addition to the selectivity of nitrogen compounds, the stoichiometric requirements of formic acid were also calculated for the nitrate reduction under both TiO_2 and Ag–TiO_2.

3. Results and discussion

3.1. Characteristics of the thin films

As shown in Fig. 2, the XRD patterns of the 0.1% Ag–TiO_2 thin films showed the prominent peaks at $2\theta = 25.2°$, the result of which confirmed the existence of the anatase phase of TiO_2 in the thin films, similar to the XRD results of the TiO_2 thin films previously reported by Rojviroon and Sirivithayapakorn [20] and to other research studies that prepared the TiO_2 catalyst in the temperature range of 400–600° (e.g. Eshaghi et al. [7], [4,25]). In addition, as witnessed in Fig. 2 the XRD patterns of Ag–TiO_2 thin films showed peaks at $2\theta = 118°$, indicating the presence of silver. Nevertheless, as the XRD results showed no distinct peaks of silver due to the low silver content, the existence of silver was thus confirmed by XRF.

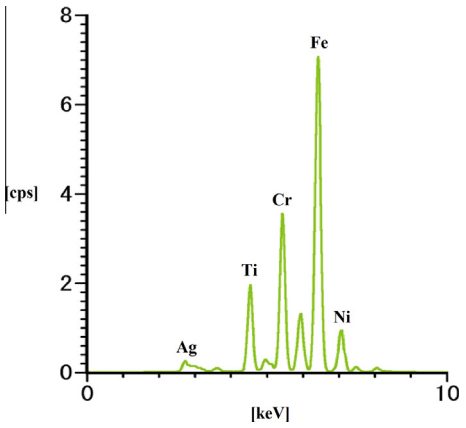

Figure 3 The XRF spectrum of 0.1% Ag–TiO_2 thin film coated on a 304 stainless steel sheet.

The XRF spectrum of the 0.1% Ag–TiO_2 thin films coated on a 304 stainless steel sheet is shown in Fig. 3. Since 304 stainless steel composes of Cr, Ni, and Fe, peaks of these elements are also present in the XRF spectrum. The presence of an Ag

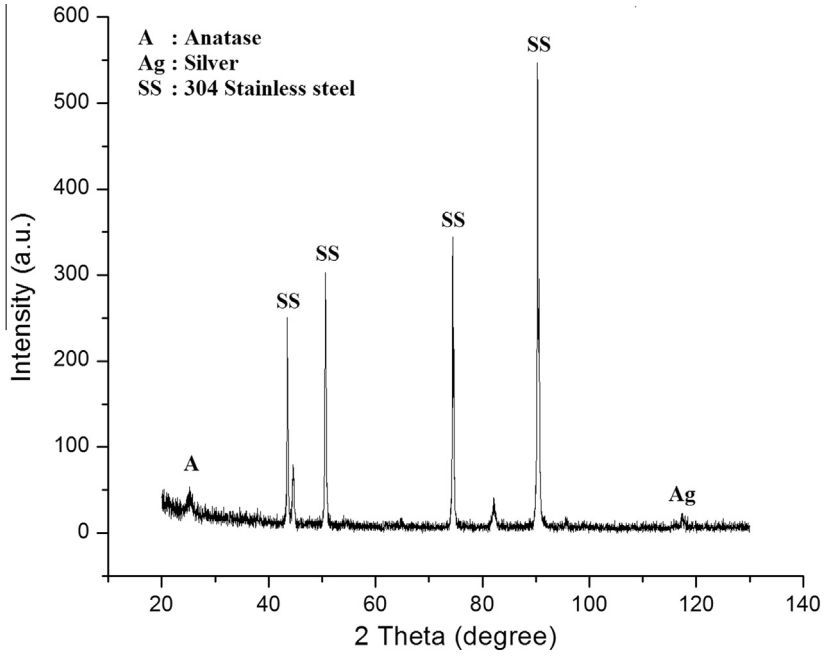

Figure 2 The XRD pattern of 0.1% Ag–TiO_2 thin films.

Table 1 Surface properties of TiO_2 thin films dip-coated on stainless steel substrates.

Surface properties	Catalysts	
	TiO_2	0.1% Ag–TiO_2
Crystalline phase of TiO_2	Anatase	Anatase
Optical band gap, (eV)	3.24	2.70
Range of grain size, (nm)	20–250	20–150
RMS average roughness, (nm)	18.25	10.96
Apparent surface area, ($m^2\ m^{-2}$) ❶	1.09	1.06
Total weight of TiO_2 on substrate, ($g\ m^{-2}$) ❷	0.16	0.13
Total apparent surface area per total weight of TiO_2, ($m^2\ g^{-1}$) ❸ = ❶/❷	6.81	8.15
Contact angle (degrees) ($\bar{x} \pm$ **SD**; $n = 5$)	94.8 ± 1.9	118.5 ± 1.1

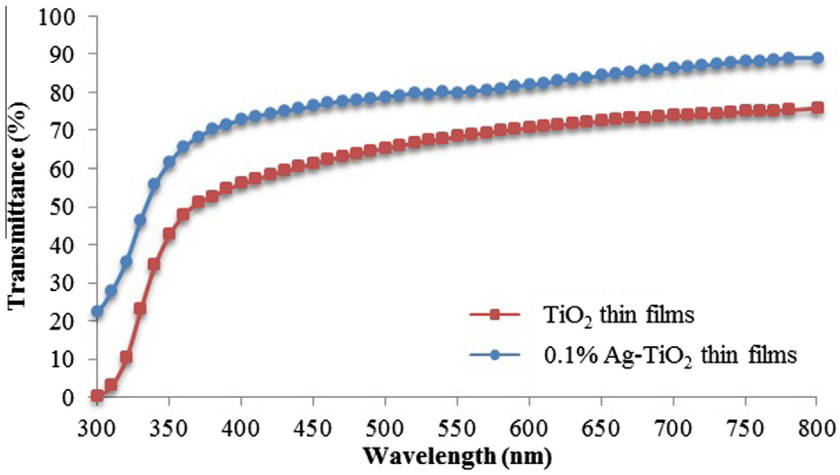

Figure 4 The transmittance spectra of the TiO_2 thin films and 0.1% Ag–TiO_2 thin films.

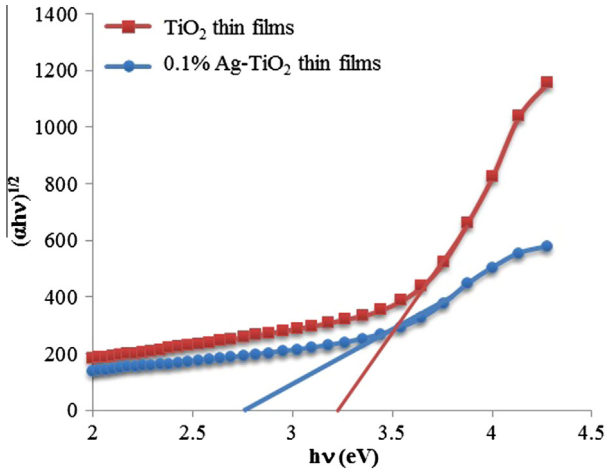

Figure 5 Optical direct band gaps (Tauc plot) of the TiO_2 thin films and 0.1% Ag–TiO_2 thin films.

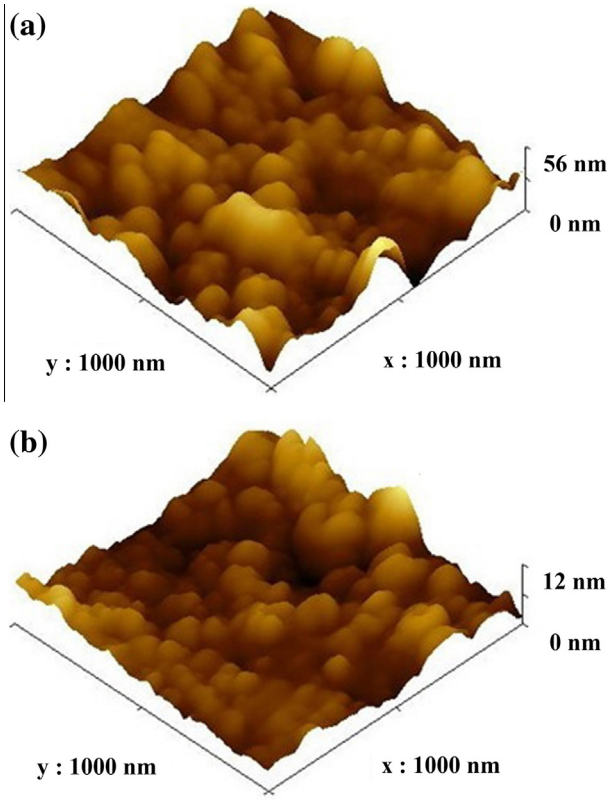

Figure 6 AFM 3D images of the thin films on stainless steel sheets: (a) TiO_2, (b) 0.1% Ag–TiO_2.

peak confirmed the successful loading of Ag onto the TiO_2 thin films.

The optical band gaps for the thin films are presented in Table 1 which are analyzed by DRS (Fig. 4) and Tanc plot (Fig. 5). As the band gap of anatase is 3.2 eV, the structure of TiO_2 in the thin films, according to the result, was anatase. The presence of Ag in the TiO_2 thin films greatly enhanced the visible light transmission (increase absorption) (Fig. 4), while narrowing the band gap from 3.24 eV to 2.70. The reason of band gap decreasing could be due to a localized surface plasmon resonance (LSPR) that was attributed by the silver nanoparticles [6]. Therefore, the actual band gap of the TiO_2 was the same, but it was the LSPR that added visible light absorbance. A similar effect on the band gap was also reported by Zhang et al. [24].

The 3D images taken with AFM of the TiO_2 and 0.1% Ag–TiO_2 thin films on stainless steel sheets are shown in Fig. 6a and b, respectively. Data on surface morphology are summarized in Table 1. Overall, the range of grain size was narrower for 0.1% Ag–TiO_2 in comparison to that of TiO_2, while the apparent surface areas of all thin films are within the same ranges. The similar effects of silver loading on grain size have been reported by He et al. [10], Bahadur et al. [2], and Liu et al. [13].

The results for water contact angles on the surface of both films as presented in Table 1 indicate that the Ag–TiO_2 thin films were more hydrophobic than the TiO_2 thin films. For the metal-doped TiO_2 thin films coated on the surface of stainless steel, several studies showed that the water contact angle tends to increase ([11,16] and [19]).

3.2. Catalytic reduction of nitrates

3.2.1. Effect of silver-doped TiO_2

Fig. 7 shows the enhanced photocatalytic activity of the Ag–TiO_2 films compared with that of the normal TiO_2 films. The data show that the concentrations of nitrate decreased from 7.14 to 3.87 mM in the TiO_2 system and from 7.14 to 1.83 mM in the Ag–TiO_2 system, equivalent to the removal efficiency of 45.8% and 74.4%, respectively. However, the concentrations of nitrate slightly decreased from 7.14 to 6.82 mM in the system of uncoated stainless steel sheets, equivalent to a mere 4.4% reduction. Therefore, the net removal of nitrate of the thin films was 41.4% and 70.0%, for TiO_2 and 0.1% Ag–TiO_2, respectively. The calculations of the reaction kinetics as a function of photon fluence according to the method described by Doudrick et al. [6] showed that the reaction rate constants were 0.14 cm^2/photons $\times 10^{14}$ for TiO_2 thin films and 0.33 cm^2/photons $\times 10^{14}$ for the 0.1% Ag–TiO_2 thin films (Table 2).

The formate removal also exhibited a similar pattern to the nitrate removal. The highest removal of formate was found in the system with 0.1% Ag–TiO_2 thin films (Fig. 7). In addition, the results confirmed the excess of formate in all experiments, indicating that the conversion of nitrate in these experiments was not restricted by the amount of formate. Similar finding was also reported by Kim and Anderson [12] during the initial period of the experiment when formate was still available in excess amount.

3.2.2. Nitrogen compounds selectivity

The concentrations of nitrite and ammonium, both of which are the aqueous by-products of the photocatalytic nitrate reduction, are shown in Fig. 8. With the progression of the reactions, the concentrations of both nitrite and ammonium slowly increased. However, the highest concentration levels of nitrite and ammonium were in the range of 1.5×10^{-2}–2.8×10^{-2} and 2.5×10^{-3}–5.2×10^{-3} mM, respectively, thereby indicating that both by-products were the intermediates of the reactions and were readily converted into the final product, i.e. the nitrogen gas [6,18].

This research study assumed that there is no N_2O generation [6]. Since very small amount of nitrite was detected in the proposed system, we assumed gas selectivity was all N_2.

Based on the selectivity (Table 2), the results indicate that the photocatalytic reduction of nitrate under both TiO_2 and Ag–TiO_2 occurred in the same fashion as previously presented by Zhang et al. [24] and Doudrick et al. [6].

3.2.3. Stoichiometric requirements of formic acid

According to the photocatalytic nitrate reduction mechanisms proposed by Rengaraj and Li [18], Lozovskii et al. [14] and

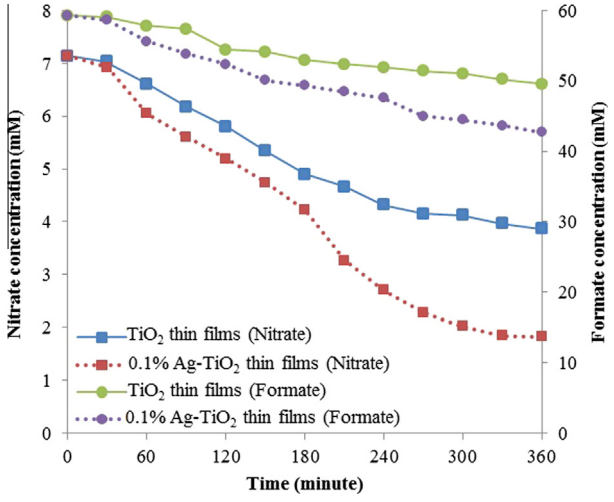

Figure 7 Removal of nitrate and formate in the system of TiO_2 thin films and 0.1% Ag–TiO_2 thin films.

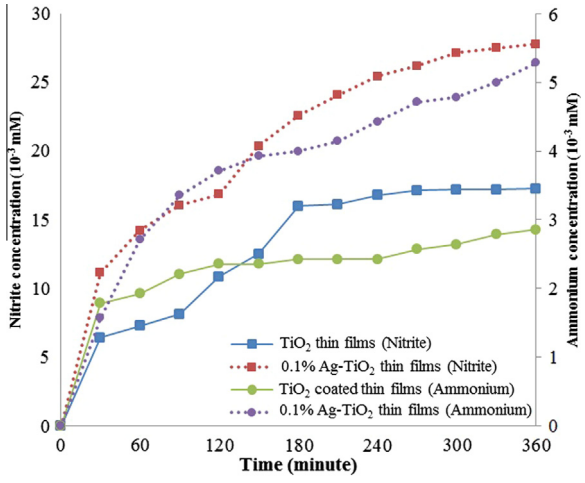

Figure 8 Concentration profiles of nitrite and ammonium in the system of TiO_2 thin films and 0.1% Ag–TiO_2 thin films.

Table 2 pH, net nitrate conversion and selectivity of nitrogen compounds.

Catalyst	Initial pH/ final pH	Net nitrate conversion (%)	Final NO_2^- selectivity (%)	Final NH_4^+ selectivity (%)	Final N_2 † selectivity (%)	Rate constant ‡ (cm^2/photons $\times 10^{14}$)
Blank *	2.75/3.25	4.4	0.29	0.16	99.6	0.01
TiO_2	2.76/3.40	41.4	0.53	0.09	99.4	0.14
0.1% Ag–TiO_2	2.75/3.74	70.0	0.52	0.10	99.4	0.33

Condition: 4.5 L solution, 100 ppm-NO_3^-N (7.14 mM), 0.1 g/L catalyst, stirring rate 60 rpm, formic acid ~59 mM, three 15 W UV black-light bulbs and continuously flushed with N_2.

† Calculated from nitrogen compounds molar balance, assuming that no N_2O is formed.

‡ The black light lamp irradiance is approximately at 370 nm.

* Uncoated stainless steel sheet.

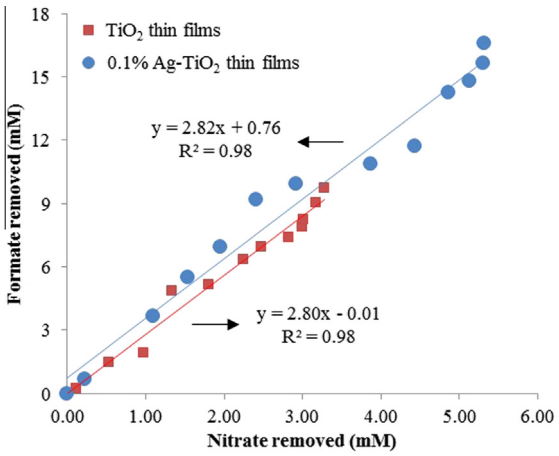

Figure 9 Relationships between moles of formate removal and nitrate removal in the system of TiO_2 thin films and 0.1% Ag–TiO_2 thin films.

Doudrick et al. [6], there exist two reaction pathways. In the first pathway, nitrate would be reduced to nitrite, which then being reduced to nitrogen gas and nitrogen gas is reduced to ammonium. This process requires 8 mol of formate to reduce 1 mol of nitrate (Rengaraj and Li [18]). Meanwhile, in the second pathway, nitrate would be reduced to nitrite and then to nitrogen gas, the process requires 2.5 mol of formate to reduce 1 mol of nitrate (Lozovskii et al. [14]; Doudrick et al. [6]). Since both nitrite and ammonium were detected in this current research work, it is likely that both pathways occurred concurrently. After obtaining the net formate removal by accounting for the formate loss in the control experiments, stoichiometric ratios of formate to nitrate in all experiments were approximately 2.8:1.0 (Fig. 9). The stoichiometric ratio of formate to nitrate in our experiments was closer to 2.5:1.0, as shown in Eq. (5). Lozovskii et al. [14] and Doudrick et al. [6] reported that the reduction of nitrate to nitrite and then to nitrogen gas could be described by Eqs. (6) and (7), the summation of which would yield Eq. (5). Therefore, with the existing nitrite and the calculated stoichiometric ratio, the main nitrate reduction reaction in this study could be that described by Eq. (5). In addition, the results showed that the loading of metal had an impact on the nitrate removal efficiency but not on the stoichiometric ratio of formate to nitrate. This thus indicated that the reaction pathways under all conditions could be identical.

$$2NO_3^- + 5HCOO^- + 7H^+ = N_2 + 5CO_2 + 6H_2O \quad (5)$$

$$NO_3^- + HCOO^- + H^+ = NO_2^- + CO_2 + H_2O \quad (6)$$

$$2NO_2^- + 3HCOO^- + 5H^+ = N_2 + 3CO_2 + 4H_2O \quad (7)$$

4. Conclusion

The prepared TiO_2 and Ag–TiO_2 thin films possess the desirable physical properties of anatase crystalline structure, nano-sized grains and hydrophobicity, thus rendering them suitable for application as catalysts in the photocatalytic processes. Under the experimental conditions in this study, the highest reaction rate constant was 0.33 cm^2/photons $\times 10^{14}$ for the 0.1% Ag–TiO_2 thin films. Moreover, nitrite and ammonium were the common intermediates found in all experiments. The presence of nitrite and the consumption of formate confirmed that the main mechanism of nitrate removal was the reduction of nitrate to nitrite and then to nitrogen gas. The loading of silver could affect the nitrate removal efficiency but had no effect on the reaction pathways.

Acknowledgements

The researchers would like to express their sincere gratitude to the Graduate School of Kasetsart University, Bangkok, Thailand, for the financial support, without which this research work would not have been materialized.

References

[1] J.A. Anderson, Photocatalytic nitrate reduction over Au/TiO_2, Catal. Today 175 (2011) 316–321.
[2] N. Bahadur, K. Jain, R. Pasricha, Govind, S. Chand, Selective gas sensing response from different loading of Ag in sol–gel mesoporous titania powders, Sens. Actuators, B 159 (2011) 112–120.
[3] E. Barajas-Ledesma, M.L. García-Benjume, I. Espitia-Cabrera, M. Ortiz-Gutiérrez, F.J. Espinoza-Beltrán, J. Mostaghimi, M.E. Contreras-García, Determination of the band gap of TiO_2–Al_2O_3 films as a function of processing parameters, Mater. Sci. Eng. B 174 (1–3) (2010) 71–73.
[4] V.G. Bessergenev, M.C. Mateus, D.A. Vasconcelos, J.F.M.L. Mariano, A.M. Botelho do Rego, R. Lange, E. Burkel, TiO_2:(Fe, S) thin films prepared from complex precursors by CVD, physical chemical properties, and photocatalysis, Int. J. Photoenergy 2012 (2012) 12. Article ID 767054.
[5] K. Doudrick, O. Monzón, A. Mangonon, K. Hristovski, P. Westerhoff, Nitrate reduction in water using commercial titanium dioxide photocatalysts (P25, P90, and Hombikat UV100), ASCE J. Environ. Eng. 138 (2012) 852–861.
[6] K. Doudrick, T. Yang, K. Hristovski, P. Westerhoff, Photocatalytic nitrate reduction in water: managing the hole scavenger and reaction by-product selectivity, Appl. Catal. B 136–137 (2013) 40–47.
[7] A. Eshaghi, R. Mozaffarinia, M. Pakshir, A. Eshaghi, Photocatalytic properties of TiO_2 sol–gel modified nanocomposite films, Ceram. Int. 37 (2011) 327–331.
[8] L. Ge, M. Xu, H. Fang, Photo-catalytic degradation of methyl orange and formaldehyde by Ag/InVO4-TiO2 thin films under visible-light irradiation, J. Mol. Catal. A 258 (1–2) (2006) 68–76.
[9] K. Hashimoto, H. Irie, A. Fujishima, TiO_2 photocatalysis: a historical overview and future prospects, Jpn. J. Appl. Phys. 44 (12) (2005) 8269–8285.
[10] C. He, Y. Yu, X. Hu, A. Larbot, Influence of silver doping on the photocatalytic activity of titania films, Appl. Surf. Sci. 200 (2002) 239–247.
[11] H. Kang, C.S. Lee, D.Y. Kim, J. Kim, W. Choi, H. Kim, Photocatalytic effect of thermal atomic layer deposition of TiO_2 on stainless steel, Appl. Catal. B 104 (2011) 6–11.
[12] D.H. Kim, M.A. Anderson, Solution factors affecting the photocatalytic and photoelectrocatalytic degradation of formic acid using supported TiO_2 thin films, J. Photochem. Photobiol. A 94 (1996) 221–229.
[13] H. Liu, X. Dong, G. Li, X. Su, Z. Zhu, Synthesis of C, Ag co-modified TiO_2 photocatalyst and its application in waste water purification, Appl. Surf. Sci. 271 (2013) 276–283.
[14] A.V. Lozovskii, I.V. Stolyarova, R.V. Prikhod'ko, V.V. Goncharuk, Research of photocatalytic activity of the Ag/TiO_2 catalysts in the reduction reaction of nitrate-ions in aqueous media, J. Water Chem. Technol. 31 (6) (2009) 360–366.

[15] G. Marci, M. Addamo, V. Augugliaro, S. Coluccia, E. Garcia-López, V. Loddo, G. Martra, L. Palmisano, M. Schiavello, Photocatalytic oxidation of toluene on irradiated TiO_2: comparison of degradation performance in humidified air, in water and in water containing a zwitterionic surfactant, J. Photochem. Photobiol. A 160 (2003) 105–114.
[16] S.H. Nam, S.J. Cho, C.K. Jung, J.H. Boo, J. Šícha, D. Heřman, J. Musil, J. Vlček, Comparison of hydrophilic properties of TiO_2 thin films prepared by sol–gel method and reactive magnetron sputtering system, Thin Solid Films 519 (2011) 6944–6950.
[17] N. Negishi, F. He, S. Matsuzawa, K. Takeuchi, K. Ohno, Waveguide type photoreactor for water purification, C. R. Chim. 9 (2006) 822–828.
[18] S. Rengaraj, X.Z. Li, Enhanced photocatalytic reduction reaction over Bi^{3+}–TiO_2 nanoparticles in presence of formic acid as a hole scavenger, Chemosphere 66 (2007) 930–938.
[19] T. Rojviroon, A. Laobuthee, S. Sirivithayapakorn, Photocatalytic activity of toluene under UV-LED light with TiO_2 thin films, Int. J. Photoenergy 2012 (2012) 8. Article ID 898464.
[20] T. Rojviroon, S. Sirivithayapakorn, Properties of TiO_2 thin films prepared using sol–gel process, Surf. Eng. 29 (1) (2013) 77–80.
[21] J. Sá, C.A. Agüera, S. Gross, J.A. Anderson, Photocatalytic nitrate reduction over metal modified TiO_2, Appl. Catal. B 85 (2009) 192–200.
[22] J. Tauc, R. Grigorovici, A. Vancu, Optical properties and electronic structure of amorphous germanium, Phys. Status Solidi B 15 (1966) 627–637.
[23] J. Tauc, Optical properties and electronic structure of amorphous Ge and Si, Mater. Res. Bull. 3 (1968) 37–46.
[24] F. Zhang, R. Jin, J. Chen, C. Shao, W. Gao, L. Li, N. Guan, High photocatalytic activity and selectivity for nitrogen in nitrate reduction on Ag/TiO_2 catalyst with fine silver clusters, J. Catal. 232 (2005) 424–431.
[25] L. Zhao, J. Ran, Z. Shu, G. Dai, P. Zhai, S. Wang, Effects of calcination temperatures on photocatalytic activity of ordered titanate nanoribbon/SnO_2 films fabricated during and EPD process, Int. J. Photoenergy 2012 (2012) 7. Article ID 472958.